ACS APPLIED MATERIALS & INTERFACES

Research Article

www.acsami.org

Template-Stripped Multifunctional Wedge and Pyramid Arrays for Magnetic Nanofocusing and Optical Sensing

Shailabh Kumar,[†,‡] Timothy W. Johnson,[†,⊥] Christopher K. Wood,[§,⊥] Tao Qu,[∥,⊥] Nathan J. Wittenberg,[†] Lauren M. Otto,[†] Jonah Shaver,[†] Nicholas J. Long,[§] Randall H. Victora,[†,∥] Joshua B. Edel,[§] and Sang-Hyun Oh*[,†,‡]

[†]Department of Electrical and Computer Engineering, [‡]Department of Biomedical Engineering, and [∥]Department of Physics, University of Minnesota, Minneapolis, Minnesota 55455, United States

[§]Department of Chemistry, Imperial College London, South Kensington, SW7 2AZ London, United Kingdom

Supporting Information

ABSTRACT: We present large-scale reproducible fabrication of multifunctional ultrasharp metallic structures on planar substrates with capabilities including magnetic field nanofocusing and plasmonic sensing. Objects with sharp tips such as wedges and pyramids made with noble metals have been extensively used for enhancing local electric fields via the lightning-rod effect or plasmonic nanofocusing. However, analogous nanofocusing of magnetic fields using sharp tips made with magnetic materials has not been widely realized. Reproducible fabrication of sharp tips with magnetic as well as noble metal layers on planar substrates can enable straightforward application of their material and shape-derived functionalities. We use a template-stripping method to produce plasmonic-shell-coated nickel wedge and pyramid arrays at the wafer-scale with tip radius of curvature close to 10 nm. We further explore the magnetic nanofocusing capabilities of these ultrasharp substrates, deriving analytical formulas and comparing the results with computer simulations. These structures exhibit nanoscale spatial control over the trapping of magnetic microbeads and nanoparticles in solution. Additionally, enhanced optical sensing of analytes by these plasmonic-shell-coated substrates is demonstrated using surface-enhanced Raman spectroscopy. These methods can guide the design and fabrication of novel devices with applications including nanoparticle manipulation, biosensing, and magnetoplasmonics.

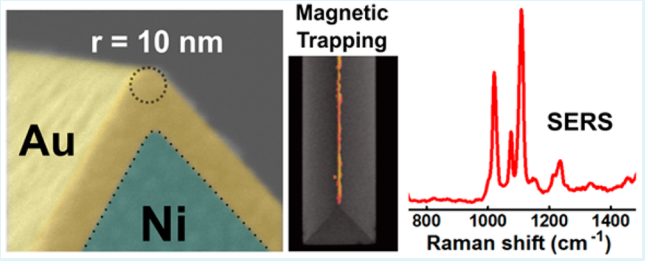

KEYWORDS: *template stripping, magnetic nanofocusing, magnetic trapping, magnetoplasmonics, SERS*

1. INTRODUCTION

Multifunctional substrates with integrated magnetic and plasmonic properties have witnessed increasing interest with applications including electromagnetic field manipulation,[1−3] enhanced molecular sensing,[4] and theranostics.[5,6] Fabrication of these multilayered materials with nanoscale features, such as ultrasharp tips, remains a desired target.[7] Nanoscale features such as sharp tips can greatly influence the distribution of electromagnetic fields around them.[8,9] Electrostatic fields near sharp conducting tips or edges exhibit a singular behavior due to the "lightning rod" effect.[10] Electromagnetic fields can also be tightly confined at sharp tips made with noble metals by "nanofocusing" incident free-space light via surface plasmons.[11,12] These properties of metallic tips have enabled various applications in near-field optical microscopy,[13,14] particle trapping,[15−18] and heat-assisted magnetic recording.[19] However, analogous applications based on sharp metallic tip-driven magnetic nanofocusing remain largely unexplored. Magnetic fields around a sharp ferromagnetic tip can far exceed the saturation magnetization of the material, leading to singular behavior near infinitely sharp tips.[20] When such ferromagnetic tips are coated with gold or silver shells, it is possible to combine strong magnetic fields with plasmonic effects. Therefore, optimal design and fabrication of ultrasharp tips with plasmonic and magnetic functionalities are highly desirable, yet reproducible, high-throughput fabrication methods have been difficult to achieve.

Among many potential applications, biosensing can greatly benefit from the aforementioned combination of enhanced magnetic and optical fields. One of the major problems in surface-based biosensing is diffusion-limited transport of analytes to the sensing surface.[21−23] This increases the time taken for detection and reduces the sensitivity for low-concentration analytes. Directed transport of analytes to the sensor surface via selective surface functionalization,[24] passive flow,[25−27] or actively using pressure-driven flow,[28] electrokinetic,[29−31] or magnetic methods[32] can improve detection sensitivity and speed. Among various options, magnetic forces

Received: December 13, 2015
Accepted: February 3, 2016
Published: February 3, 2016

DOI: 10.1021/acsami.5b12157
ACS Appl. Mater. Interfaces 2016, 8, 9319−9326

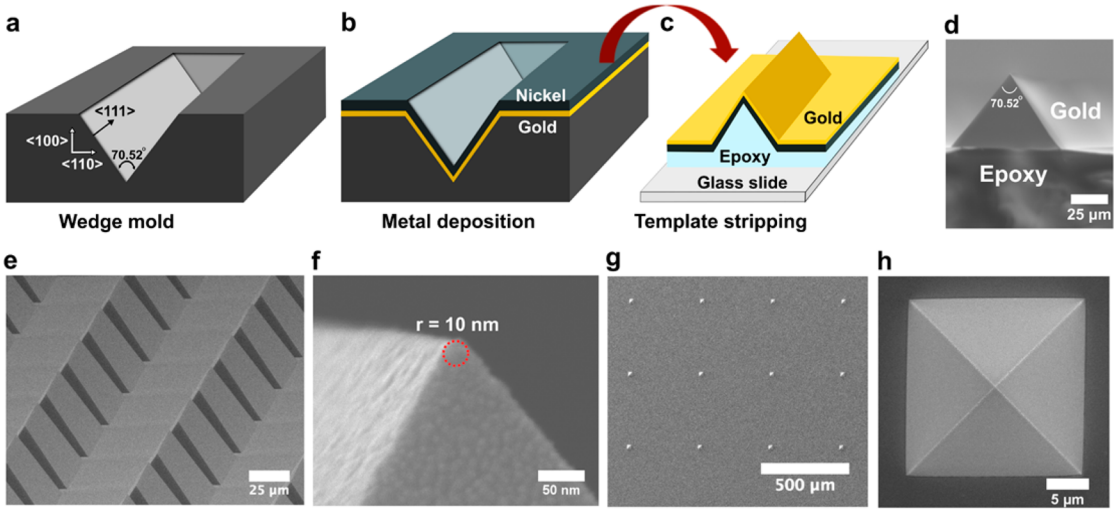

Figure 1. Fabrication scheme and SEM imaging. (a) Trenches in the silicon template formed using anisotropic etching of <100> silicon wafer in KOH. (b) Thin layer of gold followed by nickel deposited on the template using electron-beam evaporation. (c) Optical adhesive (NOA61) was added to the template and a glass slide was placed on top. The sample was then placed under ultraviolet light for curing. The metal film attached to epoxy and glass slide was template-stripped. SEM images showing (d) cross-sectional view of a template-stripped wedge. (e) bird's-eye view of arrays of wedges. (f) side-view of the tip of a wedge with 10 nm radius of curvature. This wedge had 50 nm gold deposited on top of 125 nm nickel film. (g) Widely separated array of pyramids fabricated using a pyramidal silicon template. (h) Top-down view of a template-stripped pyramid.

work well with complex media, including conductive and nontransparent solutions like blood, enabling biomedical diagnostics. The localization and enhancement of the magnetic field gradient is of great practical importance for the rapid isolation and concentration of cells or biomolecules,[33−35] which are usually tagged to magnetic beads. The ability to run multiple tests simultaneously is also important, and requires large-area substrates with arrayed sensing regions. Although magnetic tips have been produced for magnetic force microscopy (MFM) applications,[36] integration of these isolated tips with substrates for optical sensing and array-based particle manipulation is not straightforward, indicating the need for alternative fabrication techniques.

Template stripping has emerged as a practical technique to mass-produce sharp metallic wedges and pyramids with high reproducibility.[37−40] The key advantage of this approach for tip fabrication is the ability to use crystalline-orientation-dependent wet etching of silicon wafer templates[41] to produce inverted pyramids or wedges with extremely sharp corners (~10 nm radius of curvature) without using high-resolution lithography. Gold or silver deposited in these templates can be stripped out using an adhesive backing layer because of the poor adhesion between noble metals and oxidized silicon surfaces, resulting in pyramid or wedge structures with sharp tips. Non-noble metals that cannot be easily stripped from silicon templates directly can also be used in this method with the prior addition of a thin (~10 nm) layer of gold or silver on the template to enable stripping.[42] Sacrificial silicon templates have been used previously to fabricate colloids of pyramidal nickel particles and thin gold and nickel wedges[37,38,43] by dissolving the silicon templates and then recovering the devices from the aqueous solution. This fabrication process can suffer from clumping in solution (for colloidal particles), fragility (for thin wedges), and lack of template reusability.

In this work, we employ a template-stripping technique to produce sharp nickel tips with gold or silver shells on a glass substrate from a reusable silicon template. We present analytical equations, numerical simulations, and experimental evidence to demonstrate the generation of localized, extremely strong magnetic fields and field gradients near the sharp tips of these substrates. Analogous to the electrostatic lightning rod effect, the equations show that as a magnetic tip or wedge becomes infinitely sharp, the field at the tip diverges. The gold- or silver-coated nickel structures can be used for trapping magnetic nanoparticles with nanoscale control over large areas and optical analysis such as surface-enhanced Raman spectroscopy (SERS).

2. EXPERIMENTAL SECTION

Fabrication of Sharp Nickel Wedge and Pyramid Arrays. To create a silicon template for wedges, we coated standard (100) silicon wafers with 200 nm thick low-stress silicon nitride (Si_3N_4) using low-pressure chemical vapor deposition (LPCVD). Photolithography and dry etching were then used to remove nitride from the front of wafers to obtain rectangle-shaped areas with exposed silicon. The wafers were then dipped in a KOH bath where the silicon was anisotropically etched to obtain wedge-shaped grooves in silicon wafers (Figure 1a). The process for fabricating silicon templates with pyramid-shaped grooves has been described in our previous work.[40] A layer of gold or silver (thickness 10 to 50 nm) followed by a layer of nickel (thickness 125 nm) were deposited on the wafers using electron-beam evaporation (Figure 1b). The gold−nickel bilayer films were then template-stripped using optical adhesive (NOA 61, Norland Products, Inc.) and attached to a glass slide (Figure 1c).

Numerical Simulations. COMSOL Multiphysics 4.4 was used along with the AC/DC module (magnetic fields, no currents) to perform numerical simulations of several models relating to the analytical calculation and experimental conditions. A 2D approximation of a wedge was used. A Gaussmeter (GM 2, Alphalab Inc.) was used to experimentally measure the strength of the NdFeB magnet (ND040−52NM-4C, CMS magnetics, cylindrical shape with 0.5 in. diameter and 0.5 in. height) that was placed below the wedges and pyramids during experiments. The external magnetic field B was measured to be 4300 G (or 0.43 T) 1 mm above the surface of the magnet to account for the thickness of the glass slide on which the wedge and pyramids were template stripped. This magnetic field value was applied to the model by creating a magnetic potential drop vertically across the modeling region. The nickel material was modeled using a B−H curve from the available nonlinear magnetic materials in

DOI: 10.1021/acsami.5b12157
ACS Appl. Mater. Interfaces 2016, 8, 9319−9326

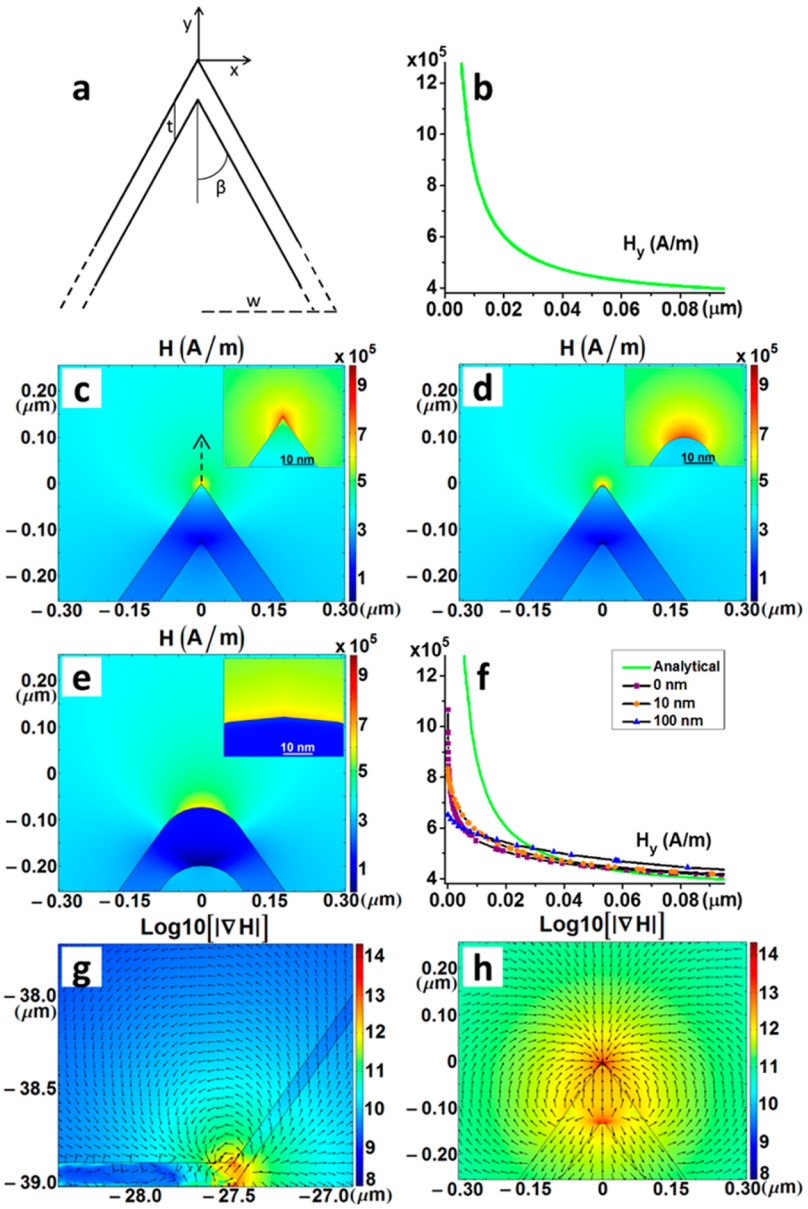

Figure 2. Analytical calculations and computational modeling results. (a) Schematic of the 2D wedge and (b) a graph of H_y as a function of the distance from the tip along the *y*-axis resulting from eq 3 + the background *H* field (342 000 A/m). COMSOL field maps of *H* in the region near the wedge tip with radius (c) 0, (d) 10, and (e) 100 nm. Insets show the area within ∼30 nm of the tip. (f) H_y as a function of the distance from the tip along the *y*-axis for both the analytical result + the background *H* field (342 000 A/m) and the modeling results corresponding to c−e (plotted along the arrow shown in c). An order of magnitude map of $|\nabla H|$, which is proportional to the strength of the force acting on a particle, is shown (g) near the base of the wedge and (h) near the 10 nm tip of the wedge. The arrows show the direction of the force (logarithmically scaled).

version 4.4. The external material (representing water, optical adhesive, and gold) was modeled as $\mu_r = 1$.

Synthesis of Silver-Coated Magnetic Polystyrene Beads. Silver-coated magnetic polystyrene beads were synthesized using a polyol reduction method with minor modifications.[44] Magnetic polystyrene beads (300 nm diameter) were obtained from Spherotech (FCM-02556−2). A small sample of beads (100 μL) were pelleted from their initial suspension (1% w/v) using a 0.5 in. diameter neodymium magnet (CMS Magnetics), then resuspended in ethylene glycol. This process was repeated, then the beads were suspended in 125 μL of ethylene glycol containing 0.25 M $AgNO_3$ and 0.35 mM polyvinylpyrrolidone-40 (PVP-40). The bead suspension was vigorously mixed with a vortex mixer then placed in an oven at 100 °C for 20 h with intermittent vortexing. After 20 h, the beads were vortexed, then sonicated for 3 min in a bath sonicator at room temperature. The beads were separated from the reaction solution by magnetic pelleting followed by discarding of the supernatant. Next the beads were resuspended in 300 μL of ethanol, triturated with a 100 μL Eppendorf pipet and vortex mixed. This process was repeated twice more, and then 700 μL of ethanol was added to make a 1 mL suspension of silver-coated magnetic polystyrene beads.

Functionalization of Silver-Coated Magnetic Polystyrene Beads. The silver-coated beads were functionalized with 4-mercaptopyridine (4-MP) as follows. In a small Eppendorf tube 180 μL of the silver-coated beads were mixed with 20 μL of a 20 mM 4-MP solution in ethanol, resulting in a final 4-MP concentration of 2 mM. The beads were incubated in this solution overnight, then washed 3 times by magnetic pelleting, discarding of supernatant, and resuspension in 200 μL of ethanol. The beads were then transferred to aqueous solution by magnetic pelleting, discarding of supernatant and resuspension in deionized water. This process was repeated two more times.

DOI: 10.1021/acsami.5b12157
ACS Appl. Mater. Interfaces 2016, 8, 9319−9326

3. RESULTS AND DISCUSSION

The process for fabricating plasmonic shell-coated sharp nickel wedges and pyramids using a template-stripping process is shown in Figure 1a–c. Glass slides with arrays of sharp metallic wedges or pyramids are obtained. A cross-sectional scanning electron micrograph (SEM) of a single wedge is shown in Figure 1d. Another SEM shows a bird's-eye view of array of wedges in Figure 1e. A zoomed-in side-view of one of the wedge tips can be seen in Figure 1f. The radius of curvature of the tip measured by SEM was approximately 10 nm. Such sharp tips were observed for 10 as well as 50 nm of deposited gold (Figure S1). Pyramids were similarly fabricated using silicon molds with pyramidal trenches (Figure 1g, h).

On account of nickel having ferromagnetic properties, the substrate can be magnetized under the influence of an external magnetic field. Substrates were magnetized using a Neodymium Iron Boron (NdFeB) magnet (ND040–52NM-4C, CMS magnetics, cylindrical shape with 0.5 in. diameter and 0.5 in. height). The degree and nature of the magnetization of the fabricated structures by the external magnetic field was explored using analytical calculations and computer simulations. First, we derived an analytical formula describing the magnetic field for an infinitely long 2D wedge with an infinitely sharp tip for the region near the tip. The cross-section of the wedge was a triangular shape with magnetic metal thickness at the tip region t, which is small compared to the base width of the triangle, as illustrated in Figure 2a.

We used the first-order Taylor expansion to obtain the magnetic scalar potential Φ_m, and the magnetic field component along the y axis, H_y.[10] For uniform saturation magnetization, the contribution to the field is only from the surface.

$$\Phi_m(0, b, 0) = \frac{M\sin(\beta)}{4\pi} \oint \frac{\partial(x^2 + (y - b)^2 + z^2)^{-1/2}}{\partial y} t dS \tag{1}$$

$$H_y(0, b, 0) = -\frac{\partial \Phi_m}{\partial b} = M\sin(\beta)\frac{w(b + w\cot(\beta))}{\pi b(w^2 + (b + w\cot(\beta))^2)} t \tag{2}$$

where b is the distance of the observation point from the tip, w is the half-width of the base of the triangular structure, β is the wedge half angle, t denotes thickness of the wedge, M is the magnetization magnitude of the wedge, and H_y is the magnetic field strength normal to the base of the structure. For points in the regions very near the tip, $b \ll w$.

$$H_y(0, b, 0) = \frac{Mt\cos(\beta)\sin^2(\beta)}{\pi b} \tag{3}$$

Using the parameter values from our fabricated wedges, assuming the magnetization to be saturated (483 000 A/m) in the vertical direction from the tip, and adding the background field from the NdFeB magnet (342 000 A/m), we calculated magnetic field strength H_y as a function of distance as shown in Figure 2b. The magnetic field rapidly decreases and is inversely proportional to the distance from the tip. It should be noted that for an infinitely sharp 2D wedge, the magnetic field H_y diverges at the tip ($b = 0$), even though the saturation magnetization and thus the effective magnetic surface charge is finite. Similarly, we can also obtain the analytic form for a 3D cone with triangular cross section, which can approximate the pyramidal tip produced via template stripping. For points very near the tip, $b \ll w$.

$$H_y(0, b, 0) = \frac{Mt\cos(\beta)\sin^2(\beta)}{b} \tag{4}$$

Comparison of eqs 3 and 4 shows that a perfectly cone-shaped 3D tip can generate a maximum field that is π times larger than the 2D wedge tip for the same tip half angle β. For template-stripped wedges and pyramids, the tip half angle β is fixed at $70.52/2 \approx 35.3°$, which is determined by the crystallographic orientation of {111} facets in silicon.[41]

To better understand the behavior of the magnetic field around the fabricated wedge structures, which has a finite radius of curvature, COMSOL Multiphysics software was used to perform numerical simulations. 2D models were created to simulate a wedge structure with varying tip radii. A 0 nm radius tip was modeled for comparison with the analytical model, a 10 nm radius tip was modeled to represent our experimental conditions, and a 100 nm radius tip was modeled for comparison with a blunt tip. Maps of the resulting fields H are shown in Figure 2c–e and become progressively weaker near the tip as the radius becomes larger (i.e., the tip becomes blunt). The dependence of H_y on the vertical distance from the tip can be seen in Figure 2f for all the three cases as well as the analytical case, after including the background field from the NdFeB magnet (342 000 A/m), which is still present in experiments. The numerical calculation for 0 nm radius suggests divergent behavior, but the power dependence of H_y on y differs from the analytic result, presumably owing to the usual numerical problems near a divergence and the lack of perfectly vertical magnetic saturation in the wedge (Figure S2).

Further calculations were performed to determine the effect of the tip geometry on the magnetic field gradient, ∇H. The tip and base regions of the wedges and pyramids have a high spatial gradient, which upon magnetization of the substrate, translates into a highly localized and strong magnetic field gradient. A base 10 logarithmic plot of ∇H generated for a 2D wedge model shows intense magnetic field gradient zones near the tip and base regions (Figure 2g, h). Figure 2g, h shows orders of magnitude difference in $|\nabla H|$ close to the wedge base and tip respectively, as compared to neighboring regions and the whole modeling window (Figure S3). The logarithmically-scaled arrows indicate the direction of force experienced by a magnetic particle in the vicinity.

Localized and intense magnetic field gradient near the sharp tips of these nanostructures can be used for rapid and directed capture of magnetic particles. Calculations based on the magnetic field gradient values obtained from computer simulations can help us realize our ability to capture magnetic nanoparticles on these substrates. Even though we have shown that the substrates can be fabricated with top metal layer thickness as low as 10 nm, we performed the calculations and trapping experiments for a system which is more relevant for plasmonic sensing, i.e., 50 nm gold or silver on top of nickel. Substrates with a minimal top metal layer covering the nickel should improve the trapping efficiency of the system, as the magnetic field and field gradient values decrease the further we move away from the nickel tip. However, thicker noble metal films are usually needed on plasmonic substrates for efficient propagation of surface plasmon polaritons (SPP) on the surface, which have a penetration depth of approximately 30 nm in gold or silver films in the visible wavelength regime.[45]

DOI: 10.1021/acsami.5b12157
ACS Appl. Mater. Interfaces 2016, 8, 9319–9326

Hence, we performed calculations for trapping of magnetic nanoparticles (300 and 30 nm diameter) on substrates with 50 nm gold and silver as the plasmonic shell.

The force on a particle with magnetic dipole $\boldsymbol{m}$ in a magnetic field can be written as

$$\mathbf{F} = \mu_0 \nabla(\boldsymbol{m}\cdot\boldsymbol{H}) \tag{5}$$

Where μ_0 is the permeability of the surrounding medium (in our case, gold and a water solution where the relative permeability ~1).[46] Because these nanoparticles are known to be superparamagnetic for our applied magnetic field of 0.43 T (field measured from the NdFeB magnet), the magnetic dipole is assumed to be saturated where $\boldsymbol{m}$ is constant and parallel to $\boldsymbol{H}$, so we can rewrite eq 5 as

$$\mathbf{F} = S\mu_0\mu_B \nabla H \tag{6}$$

Where S is the number of Bohr magnetons, μ_B. ∇H was determined from the numerical simulations (Figure 2h) to have a value of $\sim 1 \times 10^{12}$ A/m^2 in the downward direction in the region 50 nm above the tip (next to the gold), which is where the edge of a trapped particle would be located. For the 300 nm particles (FCM-02556−2, Spherotech), the composition was 12% γ-ferric oxide (γ-Fe_2O_3) by volume, which yielded $S \sim 1.5 \times 10^8$ Bohr magnetons per particle assuming 2.2 Bohr magnetons per Fe atom. As a reference, we determined the threshold force necessary to overcome Brownian motion for our 300 nm particles to be $\mathbf{F}_{th} \approx (k_B T/2r_p) = 14$ fN (k_B is Boltzmann's constant, T is the temperature (300 K), and r_p is the particle radius) whereas the force experienced by the beads 50 nm above the nickel tip was 1700 pN, thus demonstrating the simple capture of the 300 nm particles. As a rough approximation for the 30 nm particles (Nanocs Inc.), we assumed the same Fe_2O_3 properties as for the 300 nm particles and estimated the threshold force to be 0.14 pN and the applied force to be 1.7 pN. Our calculations show that even with 50 nm gold or silver layer on top of the nickel, the tip-enhanced magnetic field gradient generated by these structures should allow us to trap these nanoparticles.

For tip-enhanced magnetic trapping experiments, a drop of water containing suspended fluorescently tagged magnetic beads was placed on top of the template-stripped wedge or pyramid region. Magnetic particles of various sizes (1.6 μm, 300 nm, and 30 nm) were used for these experiments. The device was placed on an upright microscope stage and a magnet was brought in contact with the bottom surface of the glass. The larger particles (1.6 μm and 300 nm) were trapped within seconds of the application of an external magnetic field. Rough calculations showed that the applied magnetic force for the 30 nm nanoparticles was within about an order of magnitude of their threshold trapping force, and we waited about 30 min after placing the external magnet to allow for their capture. Bright-field and confocal fluorescence images were collected,[48] using a custom built microscope, for all the cases. The magnetic particles can be seen trapped at the tips (Figure 3) and base regions of the wedge structures (Figure S4). These experiments show that magnetic particles ranging from microns to tens of nanometers in diameter can be trapped on these planar glass substrates over user-defined areas of arrayed nanostructures with nanometer-scale precision. This can be performed using a droplet-based method or in combination with microfluidic channels. Many applications can be foreseen including on-chip preconcentration, spatially controlled particle assembly, and targeted delivery of molecules toward plasmonic hot spots.

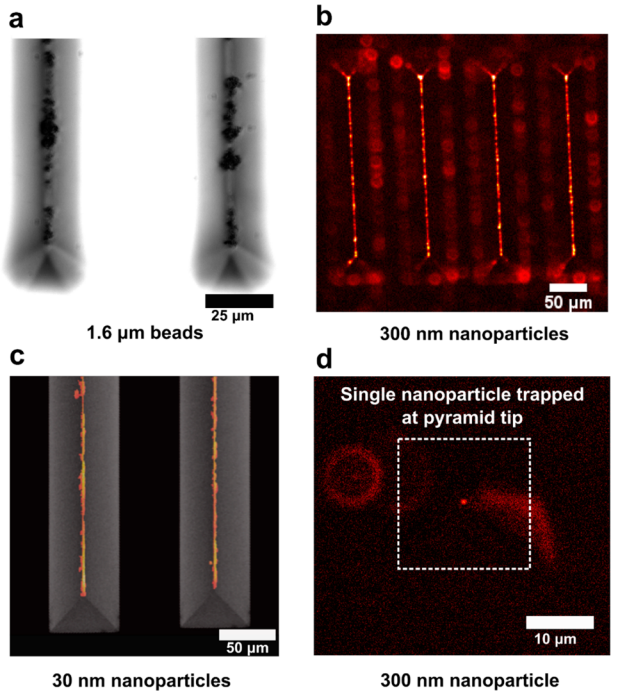

Figure 3. Tip-enhanced trapping of magnetic nanoparticles. (a) Bright-field light microscopy image showing 1.6 μm beads captured on tips of wedges. (b) Fluorescence images showing 300 nm nanoparticles captured on sharp wedge tips. (c) Fluorescence image showing 30 nm magnetic nanoparticles captured on sharp wedge tips. The image has been overlaid on top of a SEM of the wedges. (d) Fluorescence image showing capture of a single 300 nm magnetic nanoparticle at the tip of one such pyramid under the influence of a magnetic field.

Nickel pyramids were also used for magnetic trapping and it was even possible to trap a single 300 nm nanoparticle at the tip (Figure 3d). Interrogation of individual units of a system can provide further details about their behavior such as in-sample variation as compared to studying agglomerates. Trapping of individual particles is particularly important when combined with tip-based analytical sensing, giving us control over the number of analytes being interrogated by the sharp pyramidal tip. Our experimental results demonstrate tip-based trapping of magnetic nanoparticles, indicating strongly localized and enhanced magnetic fields as expected from theory and computational modeling. We can further increase the force experienced by the beads by applying stronger external magnetic fields, using materials with stronger saturation magnetization such as Co or NiFe, fabricating even sharper tips,[47] or reducing the thickness of the top gold/silver layer.

A potential application of this technique is to improve the sensitivity of plasmonic sensors. Magnetic beads tagged with analyte molecules can be concentrated on these sharp metallic tips or bases. As the wedges and pyramid substrates are coated with gold or silver, they can be used as plasmonic sensing substrates for concurrent SPR or SERS detection. To demonstrate this, we coated the 300 nm magnetic beads with layers of silver nanoparticles.[44] These beads were then tagged with 4-mercaptopyridine (4-MP), which forms a monolayer on the silver surface via covalent thiol-metal bonds (Figure 4a). These Ag-nanoparticle-coated beads were found to be excellent SERS substrates by themselves. The 4-MP tagged magnetic particles were trapped on three different substrates to test for

DOI: 10.1021/acsami.5b12157
ACS Appl. Mater. Interfaces 2016, 8, 9319−9326

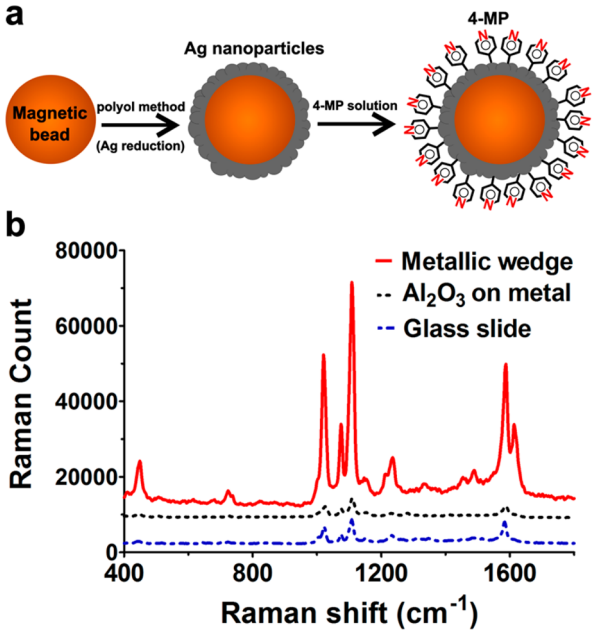

Figure 4. Plasmonic sensing using trapped silver-coated magnetic nanoparticles. (a) Cross-sectional schematic showing the chemical functionalization of magnetic beads with 4-mercaptopyridine (4-MP) after coating them with Ag nanoparticles. (b) Raman signal obtained from the beads captured on metallic wedges as compared to 10 nm of Al_2O_3-coated metallic wedges and standard glass slide.

any plasmonic contribution from the metal layer on top. The three substrates were (a) magnetic wedges coated with a 50 nm silver shell (Ag/Ni); b) magnetic wedges with a 50 nm silver shell and 10 nm Al_2O_3 (Al_2O_3/Ag/Ni); and c) a standard glass slide. Substrates b and c serve as negative controls for SERS as the 4-MP molecules have minimal or no interaction with the metal surface.

The results show that a higher Raman signal was obtained from the beads trapped on the silver-coated nickel wedges as compared to those on glass slides or Al_2O_3-coated wedges (Figure 4b). The signal intensities obtained from glass slides and Al_2O_3-coated wedge substrates were very similar, which is expected, as there is no enhancement from the substrate. For the particles captured on silver-coated wedges, the observed enhancement could be a result of generation of hotspots, which are nanoscale regions of intense electromagnetic field, between the wedge metal layer and silver nanoparticles on the magnetic beads.[49] The observed Raman enhancement is expected to be much higher if the trapped beads were not excellent SERS substrates themselves. The moderate SERS enhancement could also be a result of weak collection efficiency from the plasmonic hotspots on the wedge surface. For further Raman applications, plasmonic nanofocusing could be utilized to launch and confine surface plasmons at the sharp tips.[11−13,50] Furthermore, these tips can combine strong magnetic fields and plasmonic hot spots for novel applications in magnetoplasmonics.

4. CONCLUSION

In summary, we have fabricated large-area multifunctional wedge and pyramid arrays directly onto planar substrates via template stripping. The integrated capabilities of these structures toward magnetic nanofocusing, trapping as well as plasmonic sensing were then explored. Simple analytical equations were derived, allowing calculation of the magnitude of enhanced magnetic fields near sharp tips. COMSOL modeling revealed a similar trend for the magnetic field distribution close to the fabricated nanostructures. Tip-enhanced magnetic trapping was shown using magnetic particles ranging from microns to tens of nanometers with nanoscale control over their localization. The force experienced by magnetic particles during these experiments was also analyzed, which can help design sensors with better understanding of the rate and efficiency of magnetic nanoparticle capture. This directed trapping can be used for various applications including concentration, isolation and analysis of analytes,[51] as well as cells,[52] and viruses.[53] Compared with electrokinetic or optical trapping methods, magnetic trapping is highly advantageous for handling biological samples, as it does not suffer from restrictions based on solution transparency or conductivity and does not cause any local heating effects, which may damage the samples. The fabricated substrates with periodically arranged nanostructures over a wide area can allow multiple droplet or microfluidics based experiments on the same chip with array-like analysis.[54] Integrated microfluidics may also enable shear force-based removal of unbound or weakly bound particles from the metal surface, allowing the substrates to be reused as well as for other particle trapping and release-based applications. We also showed that these plasmonic shell coated structures can be applied for optical sensing such as SERS. Future directions include applying these nanostructures for magnetic-field-aided optical[55] and electrochemical sensing.[56]

■ ASSOCIATED CONTENT

Supporting Information

The Supporting Information is available free of charge on the ACS Publications website at DOI: 10.1021/acsami.5b12157.

Images showing fabricated tip, simulated magnetization of the substrate, and particle trapping (PDF)

■ AUTHOR INFORMATION

Corresponding Author

*E-mail: sang@umn.edu.

Author Contributions

⊥T.W.J., C.K.W., and T.Q. contributed equally to this work.

Notes

The authors declare no competing financial interest.

■ ACKNOWLEDGMENTS

This work was supported by grants from the National Science Foundation (NSF CAREER Award for S.K., N.J.W., L.M.O., S.H.O.; NSF Graduate Research Fellowship for L.M.O.), Seagate Technology through the Center for Micromagnetics and Information Technologies (MINT) at the University of Minnesota (J.S., T.Q., S.H.O., R.H.V.), EPSRC (J.B.E., C.K.W., and N.J.L.), ERC (J.B.E.), and the MnDrive Initiative (N.J.W. and S.H.O). S.H.O. also acknowledges the NSF program: Research Opportunities in Europe for NSF CAREER awardees (DBI 1338654), which supported this collaboration between the University of Minnesota and Imperial College London. S.K. was supported by the Doctoral Dissertation Fellowship from the University of Minnesota. Device fabrication was performed at the Minnesota Nano Center at the University of Minnesota, which receives support from the NSF through the National Nanotechnology Coordinated Infrastructure. Computational

DOI: 10.1021/acsami.5b12157
ACS Appl. Mater. Interfaces 2016, 8, 9319−9326

modeling using COMSOL Multiphysics was performed through the University of Minnesota Supercomputing Institute.

REFERENCES

(1) Temnov, V. V.; Armelles, G.; Woggon, U.; Guzatov, D.; Cebollada, A.; Garcia-Martin, A.; Garcia-Martin, J.; Thomay, T.; Leitenstorfer, A.; Bratschitsch, R. Active Magneto-Plasmonics in Hybrid Metal−Ferromagnet Structures. *Nat. Photonics* **2010**, *4*, 107−111.

(2) Belotelov, V. I.; Akimov, I. A.; Pohl, M.; Kotov, V. A.; Kasture, S.; Vengurlekar, A. S.; Gopal, A. V.; Yakovlev, D. R.; Zvezdin, A. K.; Bayer, M. Enhanced Magneto-Optical Effects in Magnetoplasmonic Crystals. *Nat. Nanotechnol.* **2011**, *6*, 370−376.

(3) Banthi, J. C.; Meneses-Rodriguez, D.; Garcia, F.; Gonzalez, M. U.; Garcia-Martin, A.; Cebollada, A.; Armelles, G. High Magneto-Optical Activity and Low Optical Losses in Metal-Dielectric Au/Co/Au−SiO2Magnetoplasmonic Nanodisks. *Adv. Mater.* **2012**, *24*, OP36−OP41.

(4) Regatos, D.; Sepulveda, B.; Farina, D.; Carrascosa, L. G.; Lechuga, L. M. Suitable Combination of Noble/Ferromagnetic Metal Multilayers for Enhanced Magneto-Plasmonic Biosensing. *Opt. Express* **2011**, *19*, 8336−8346.

(5) Chen, W.; Xu, N.; Xu, L.; Wang, L.; Li, Z.; Ma, W.; Zhu, Y.; Xu, C.; Kotov, N. A. Multifunctional Magnetoplasmonic Nanoparticle Assemblies for Cancer Therapy and Diagnostics (Theranostics). *Macromol. Rapid Commun.* **2010**, *31*, 228−236.

(6) Hoskins, C.; Min, Y.; Gueorguieva, M.; McDougall, C.; Volovick, A.; Prentice, P.; Wang, Z.; Melzer, A.; Cuschieri, A.; Wang, L. Hybrid Gold-Iron Oxide Nanoparticles as a Multifunctional Platform for Biomedical Application. *J. Nanobiotechnol.* **2012**, *10*, 27.

(7) Zhou, H.; Kim, J.-P.; Bahng, J. H.; Kotov, N. A.; Lee, J. Self-Assembly Mechanism of Spiky Magnetoplasmonic Supraparticles. *Adv. Funct. Mater.* **2014**, *24*, 1439−1448.

(8) Maier, S. A. *Plasmonics: Fundamentals and Applications*; Springer: New York, 2007.

(9) Halas, N. J.; Lal, S.; Chang, W. S.; Link, S.; Nordlander, P. Plasmons in Strongly Coupled Metallic Nanostructures. *Chem. Rev.* **2011**, *111*, 3913−3961.

(10) Jackson, J. D. *Classical Electrodynamics*, 3rd ed.; Wiley: New York, 1998.

(11) Stockman, M. I. Nanofocusing of Optical Energy in Tapered Plasmonic Waveguides. *Phys. Rev. Lett.* **2004**, *93*, 137404.

(12) Gramotnev, D. K.; Bozhevolnyi, S. I. Plasmonics Beyond the Diffraction Limit. *Nat. Photonics* **2010**, *4*, 83−91.

(13) Novotny, L.; Hecht, B. *Principles of Nano-optics*, 2nd ed.; Cambridge University Press: Cambridge, U.K., 2012.

(14) Novotny, L.; Van Hulst, N. Antennas for Light. *Nat. Photonics* **2011**, *5*, 83−90.

(15) Novotny, L.; Bian, R. X.; Xie, X. S. Theory of Nanometric Optical Tweezers. *Phys. Rev. Lett.* **1997**, *79*, 645−648.

(16) Xu, H.; Käll, M. Surface-Plasmon-Enhanced Optical Forces in Silver Nanoaggregates. *Phys. Rev. Lett.* **2002**, *89*, 246802.

(17) Pang, Y.; Gordon, R. Optical Trapping of a Single Protein. *Nano Lett.* **2012**, *12*, 402−406.

(18) Jose, J.; Kress, S.; Barik, A.; Otto, L. M.; Shaver, J.; Johnson, T. W.; Lapin, Z. J.; Bharadwaj, P.; Novotny, L.; Oh, S.-H. Individual Template-Stripped Conductive Gold Pyramids for Tip-Enhanced Dielectrophoresis. *ACS Photonics* **2014**, *1*, 464−470.

(19) Challener, W. A.; Peng, C.; Itagi, A. V.; Karns, D.; Peng, W.; Peng, Y.; Yang, X.; Zhu, X.; Gokemeijer, N. J.; Hsia, Y.-T.; Ju, G.; Rottmayer, R. E.; Seigler, M. A.; Gage, E. C. Heat-Assisted Magnetic Recording by a Near-Field Transducer with Efficient Optical Energy Transfer. *Nat. Photonics* **2009**, *3*, 220−224.

(20) Van Bladel, J. Field Singularities At the Tip of a Cone. *Proc. IEEE* **1983**, *71*, 901−902.

(21) Sheehan, P. E.; Whitman, L. M. Detection Limits for Nanoscale Biosensors. *Nano Lett.* **2005**, *5*, 803−807.

(22) Squires, T. M.; Messinger, R. J.; Manalis, S. R. Making It Stick: Convection, Reaction and Diffusion in Surface-Based Biosensors. *Nat. Biotechnol.* **2008**, *26*, 417−426.

(23) Feuz, L.; Jönsson, P.; Jonsson, M. P.; Höök, F. Improving the Limit of Detection of Nanoscale Sensors by Directed Binding to High-Sensitivity Areas. *ACS Nano* **2010**, *4*, 2167−2177.

(24) Jonsson, M. P.; Dahlin, A. B.; Feuz, L.; Petronis, S.; Höök, F. Locally Functionalized Short-Range Ordered Nanoplasmonic Pores for Bioanalytical Sensing. *Anal. Chem.* **2010**, *82*, 2087−2094.

(25) Kumar, S.; Wittenberg, N. J.; Oh, S.-H. Nanopore-Induced Spontaneous Concentration for Optofluidic Sensing and Particle Assembly. *Anal. Chem.* **2013**, *85*, 971−977.

(26) Kumar, S.; Cherukulappurath, S.; Johnson, T. W.; Oh, S.-H. Millimeter-Sized Suspended Plasmonic Nanohole Arrays for Surface-Tension-Driven Flow-Through SERS. *Chem. Mater.* **2014**, *26*, 6523−6530.

(27) Turek, V. A.; Francescato, Y.; Cadinu, P.; Crick, C. R.; Elliott, L.; Chen, Y.; Urland, V.; Ivanov, A. P.; Velleman, L.; Hong, M.; Vilar, R. Self-Assembled Spherical Supercluster Metamaterials from Nanoscale Building Blocks. *ACS Photonics* **2016**, *3*, 35−42.

(28) Eftekhari, F.; Escobedo, C.; Ferreira, J.; Duan, X.; Girotto, E. M.; Brolo, A. G.; Gordon, R.; Sinton, D. Nanoholes As Nanochannels: Flow-through Plasmonic Sensing. *Anal. Chem.* **2009**, *81*, 4308−4311.

(29) Escobedo, C.; Brolo, A. G.; Gordon, R.; Sinton, D. Optofluidic Concentration: Plasmonic Nanostructure as Concentrator and Sensor. *Nano Lett.* **2012**, *12*, 1592−1596.

(30) Barik, A.; Otto, L. M.; Yoo, D.; Jose, J.; Johnson, T. W.; Oh, S.-H. Dielectrophoresis-Enhanced Plasmonic Sensing with Gold Nanohole Arrays. *Nano Lett.* **2014**, *14*, 2006−2012.

(31) Freedman, K. J.; Otto, L. M.; Ivanov, A. P.; Barik, A.; Oh, S.-H.; Edel, J. B. Nanopore sensing at ultra-low concentrations using single-molecule dielectrophoretic trapping. *Nat. Commun.* **2016**, *7*, 10217.

(32) Soelberg, S. D.; Stevens, R. C.; Limaye, A. P.; Furlong, C. E. Surface Plasmon Resonance Detection Using Antibody-Linked Magnetic Nanoparticles for Analyte Capture, Purification, Concentration, and Signal Amplification. *Anal. Chem.* **2009**, *81*, 2357−2363.

(33) Deng, T.; Prentiss, M.; Whitesides, G. M. Fabrication of Magnetic Microfiltration Systems Using Soft Lithography. *Appl. Phys. Lett.* **2002**, *80*, 461−463.

(34) Pamme, N.; Wilhelm, C. Continuous Sorting of Magnetic Cells via On-Chip Free-Flow Magnetophoresis. *Lab Chip* **2006**, *6*, 974−980.

(35) Lou, X.; Qian, J.; Xiao, Y.; Viel, L.; Gerdon, A. E.; Lagally, E. T.; Atzberger, P.; Tarasow, T. M.; Heeger, A. J.; Soh, H. T. Micromagnetic Selection of Aptamers In Microfluidic Channels. *Proc. Natl. Acad. Sci. U. S. A.* **2009**, *106*, 2989−2994.

(36) Futamoto, M.; Hagami, T.; Ishihara, S.; Soneta, K.; Ohtake, M. Improvement of Magnetic Force Microscope Resolution and Application to High-Density Recording Media. *IEEE Trans. Magn.* **2013**, *49*, 2748−2754.

(37) Henzie, J.; Kwak, E. S.; Odom, T. W. Mesoscale Metallic Pyramids with Nanoscale Tips. *Nano Lett.* **2005**, *5*, 1199−1202.

(38) Boltasseva, A.; Volkov, V. S.; Nielsen, R. B.; Moreno, E.; Rodrigo, S. G.; Bozhevolnyi, S. I. Triangular Metal Wedges for Subwavelength Plasmon-Polariton Guiding at Telecom Wavelengths. *Opt. Express* **2008**, *16*, 5252−5260.

(39) Nagpal, P.; Lindquist, N. C.; Oh, S.-H.; Norris, D. J. Ultrasmooth Patterned Metals for Plasmonics and Metamaterials. *Science* **2009**, *325*, 594−597.

(40) Johnson, T. W.; Lapin, Z. J.; Beams, R.; Lindquist, N. C.; Rodrigo, S. G.; Novotny, L.; Oh, S.-H. Highly Reproducible Near-Field Optical Imaging with Sub-20-nm Resolution Based on Template-Stripped Gold Pyramids. *ACS Nano* **2012**, *6*, 9168−9174.

(41) Lindquist, N. C.; Nagpal, P.; McPeak, K. M.; Norris, D. J.; Oh, S.-H. Engineering Metallic Nanostructures for Plasmonics And Nanophotonics. *Rep. Prog. Phys.* **2012**, *75*, 036501.

(42) Park, J. H.; Nagpal, P.; McPeak, K. M.; Lindquist, N. C.; Oh, S.-H.; Norris, D. J. Fabrication of Smooth Patterned Structures of Refractory Metals, Semiconductors, and Oxides via Template Stripping. *ACS Appl. Mater. Interfaces* **2013**, *5*, 9701−9708.

DOI: 10.1021/acsami.5b12157
ACS Appl. Mater. Interfaces 2016, 8, 9319−9326

(43) Lee, J.; Hasan, W.; Lee, M. H.; Odom, T. W. Optical Properties and Magnetic Manipulation of Bimaterial Nanopyramids. *Adv. Mater.* **2007**, *19*, 4387−4391.
(44) Jun, B.-H.; Noh, M. S.; Kim, G.; Kang, H.; Kim, J. H.; Chung, W.-J.; Kim, M.-S.; Kim, Y.-K.; Cho, M. H.; Jeong, D. H.; Lee, Y. S. Protein Separation and Identification Using Magnetic Beads Encoded with Surface-Enhanced Raman Spectroscopy. *Anal. Biochem.* **2009**, *391*, 24−30.
(45) Homola, J.; Yee, S. S.; Gauglitz, G. Surface Plasmon Resonance Sensors: Review. *Sens. Actuators, B* **1999**, *54*, 3−15.
(46) Inglis, D. W.; Riehn, R.; Austin, R. H.; Sturm, J. C. Continuous microfluidic immunomagnetic cell separation. *Appl. Phys. Lett.* **2004**, *85*, 5093−5095.
(47) Im, H.; Oh, S.-H. Oxidation Sharpening, Template Stripping, and Passivation of Ultra-Sharp Metallic Pyramids and Wedges. *Small* **2014**, *10*, 680−684.
(48) Crick, C. R.; Noimark, S.; Peveler, W. J.; Bear, J. C.; Ivanov, A. P.; Edel, J. B.; Parkin, I. P. Advanced analysis of nanoparticle composites−a means toward increasing the efficiency of functional materials. *RSC Adv.* **2015**, *5*, 53789−53795.
(49) Ward, D. R.; Grady, N. K.; Levin, C. S.; Halas, N. J.; Wu, Y. P.; Nordlander, P.; Natelson, D. Electromigrated Nanoscale Gaps for Surface-Enhanced Raman Spectroscopy. *Nano Lett.* **2007**, *7*, 1396−1400.
(50) Cherukulappurath, S.; Johnson, T. W.; Lindquist, N. C.; Oh, S.-H. Template-Stripped Asymmetric Metallic Pyramids for Tunable Plasmonic Nanofocusing. *Nano Lett.* **2013**, *13*, 5635−5641.
(51) Grancharov, S. G.; Zeng, H.; Sun, S.; Wang, S. X.; O'Brien, S.; Murray, C. B.; Kirtley, J. R.; Held, G. A. Bio-Functionalization of Monodisperse Magnetic Nanoparticles and Their Use as Biomolecular Labels in a Magnetic Tunnel Junction Based Sensor. *J. Phys. Chem. B* **2005**, *109*, 13030−13035.
(52) Tanase, M.; Felton, E. J.; Gray, D. S.; Hultgren, A.; Chen, C. S.; Reich, D. H. Assembly of Multicellular Constructs and Microarrays of Cells Using Magnetic Nanowires. *Lab Chip* **2005**, *5*, 598−605.
(53) Chen, G. D.; Alberts, C. J.; Rodriguez, W.; Toner, M. Concentration and Purification of Human Immunodeficiency Virus Type 1 Virions by Microfluidic Separation of Superparamagnetic Nanoparticles. *Anal. Chem.* **2010**, *82*, 723−728.
(54) Ng, A. H. C.; Choi, K.; Luoma, R. P.; Robinson, J. M.; Wheeler, A. R. Digital Microfluidic Magnetic Separation for Particle-Based Immunoassays. *Anal. Chem.* **2012**, *84*, 8805−8812.
(55) Ye, X.; Chen, J.; Diroll, B. T.; Murray, C. B. Tunable Plasmonic Coupling in Self-Assembled Binary Nanocrystal Super lattices Studied by Correlated Optical Microspectrophotometry and Electron Microscopy. *Nano Lett.* **2013**, *13*, 1291−1297.
(56) Dahlin, A. B.; Dielacher, B.; Rajendran, P.; Sugihara, K.; Sannomiya, T.; Zenobi-Wong, M.; Vörös, J. Electrochemical Plasmonic Sensors. *Anal. Bioanal. Chem.* **2012**, *402*, 1773−1784.

DOI: 10.1021/acsami.5b12157
ACS Appl. Mater. Interfaces 2016, 8, 9319−9326